# A Nonlinear Model of an Ocean Driven by Wind and Differential Heating: Part II. An Analysis of the Heat, Vorticity and Energy Balance

KIRK BRYAN AND MICHAEL D. COX

*Geophysical Fluid Dynamics Laboratory, ESSA, Princeton, N. J.*

(Manuscript received 1 May 1967, in revised form 1 June 1968)

ABSTRACT

An analysis is made of the heat and vorticity balance of a numerical model of a baroclinic ocean. The computation is carried out on a three-dimensional grid designed to resolve the thermocline, and the narrow sidewall boundary layers at the coasts. A vorticity analysis indicates almost perfect geostrophic balance in the interior. In the immediate vicinity of the western wall the vorticity balance at a given level is dominated by lateral friction and vortex stretching associated with upwelling. The "beta" effect plays an important, but somewhat lesser role. A study of the heat balance in the interior shows that lateral advection is of primary importance in the upper part of the model ocean as it removes heat received at the surface in areas of wind-induced downwelling. Some of this heat is carried to the western boundary where it compensates the cooling due to upwelling and convective transfer through the surface.

An examination of the time-dependent motion indicates a regular downstream movement of eddies in the western boundary current. These eddies extend throughout the water column and give rise to a Reynolds stress which acts to retard the time-averaged flow. In a test run with bottom friction included, these eddies are slowly damped.

## 1. Introduction

Part I of this study (Bryan and Cox, 1968) describes the method and the principal results obtained in a numerical experiment with an ocean circulation model. The flow in the model is driven by a temperature gradient imposed at the surface and a surface wind stress. Spherical geometry is taken into account and the principal simplifications are the hydrostatic approximation, the Boussinesq approximation, and an implicit treatment of small-scale motions in a "turbulent viscosity" hypothesis. The ocean basin is of uniform depth, and a symmetry condition is imposed at the equator. The basin is bounded laterally by two meridians, and the 67° parallel of latitude.

The purpose of Part II of this study is to analyze the fields of motion and temperature in greater detail. In order to understand the physical processes involved, the heat, vorticity and energy balances are computed term by term. The results are intended as a check on the consistency of the numerical method and may be useful in formulating future analytical studies.

## 2. The vorticity balance

In the case of large-scale ocean currents there is a close balance between the Coriolis and pressure terms in the equations of motion. That is to say, the large-scale motions are highly geostrophic. It is therefore undesirable to base an analysis of the dynamics of large-scale ocean currents on the equations of motion themselves, since smaller terms, which are very important in determining the flow, are obscured. The vorticity equation is more suitable for this purpose since the pressure forces are eliminated. Let

$$\zeta = \nabla_2 \times \mathbf{V},$$

where $\nabla_2$ is the horizontal grad operator, and $\mathbf{V}$ is the horizontal velocity vector. Let $\mathbf{F}$ be the force exerted by lateral friction. Cross-differentiating the two equations of motion (2.24) and (2.25) of Section 2, Part I, we have

$$\mathrm{Ro}\zeta_t = \overbrace{\mathrm{Ro}(\nabla_2 \times \mathbf{F})/\mathrm{Re}}^{a} - \overbrace{v\cos\varphi}^{b} + \overbrace{w_z \sin\varphi}^{c} - \overbrace{\mathrm{Ro}[\nabla_2 \times (\mathbf{v}\nabla_2 \mathbf{v} + w\mathbf{v}_z)]}^{d} + \overbrace{\mathrm{Ro}\zeta_{zz}}^{e}. \quad (2.1)$$

Taken in order as they appear on the right-hand side of (2.1) we have: *a*, the lateral friction term; *b*, the beta term; *c*, the divergence term; *d*, the vorticity advection term; and *e*, the vertical friction term. The terms which have Ro as a coefficient are independent of rotation, while the terms *c* and *b* depend directly on rotation, and the latitudinal variation of rotation, respectively.

We will first consider the balance which exists in the interior. Fig. 1 shows an average of the vorticity balance at 28° latitude, taking into account all of the basin with the exception of the region just adjacent to the eastern and western boundary. The abscissa is the local vorticity change and the ordinate is the $Z$ coordinate. In the interior, velocity is of the order of unity, since

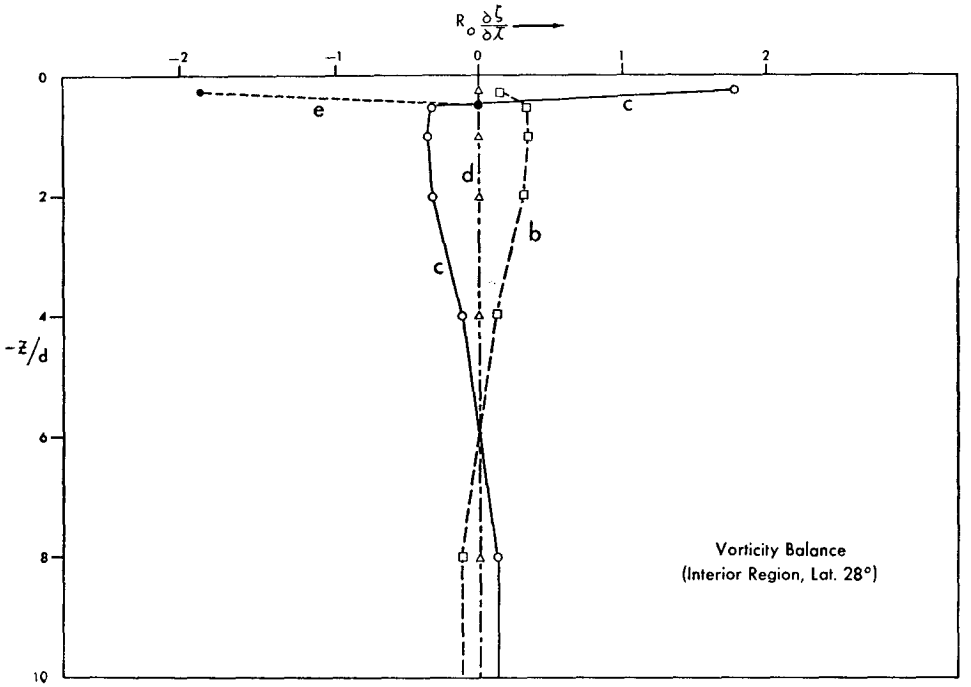


FIG. 1. The vorticity balance of the model ocean interior region in the subtropical gyre. The abscissa is local vorticity change and the ordinate is depth. Balance terms *b*, *c*, *d*, and *e*, are defined in (2.1) and in Fig. 2.

the scaling is based on interior flow. The Rossby number for the case under consideration is $2\times10^{-4}$; thus, all terms such as *a*, *d*, and *e*, in which the Rossby number appears as a coefficient, are very small indeed. Only in a surface boundary layer is the vertical friction important in causing a diffusion of anticyclonic vorticity generated by the wind down into the model ocean. Below this boundary layer there exists an almost perfect balance between *b* and *c*. Southward flow at upper levels in the subtropical gyre, and northward flow at lower levels, causes the beta term to change sign at mid-depth. In this highly geostrophic regime, the only divergence is so-called "planetary" divergence due to the change of Coriolis force with latitude.

In the western boundary current the gradients are more intense and the velocities larger than in the interior, and departures from geostrophy are important at all depths. The vorticity balance is shown in Fig. 2 for each level. Care is taken to follow the same numerical procedure as in the original calculation. The ordinate is local vorticity change in this case, and the abscissa is distance from the western boundary. The balance is no longer between the beta term and the divergence term. Except at the 4th level ($Z=-2.0$), the beta term and the divergence term are actually of the same, rather than of opposite sign. Since the boundary current is flowing northward at the surface, and southward at great depths, the drag at the west wall creates positive vorticity (counterclockwise) at the surface and negative vorticity (clockwise) at the bottom. Outflow from the wall in the surface layers (not shown) causes a transfer of the vorticity generated near the wall out into the body of the fluid.

As in the interior region, the vertical friction term is important only in the surface boundary layer. Note that the divergence term *c* is small and positive for the lower three levels and becomes large and negative right at the surface. This feature is associated with the very great upwelling which takes place right adjacent to the wall shown in Fig. 11 of Part I. The relatively weak divergence, acting through deep layers below, balances the much stronger convergence acting in shallower layers at the surface, so that the total integrated divergence vanishes. A maximum vertical velocity is found between the 3rd and 4th levels at about $Z=-1.5$. The importance of this upward velocity in maintaining the heat balance at the western wall will be shown in the following section.

### 3. The heat balance

The equation for apparent temperature is given in Part I as

$$\vartheta_t+\sec\varphi\, u\vartheta_\lambda+v\vartheta_\varphi+w\vartheta_z=(1/\delta)\vartheta_{zz}+\mathrm{P\acute{e}}^{-1}\Delta\vartheta, \quad (3.1)$$

where

$$\delta=\begin{cases}1, & \vartheta_z>0\\ 0, & \vartheta_z<0\end{cases}.$$

The heat balance will be examined by analyzing the

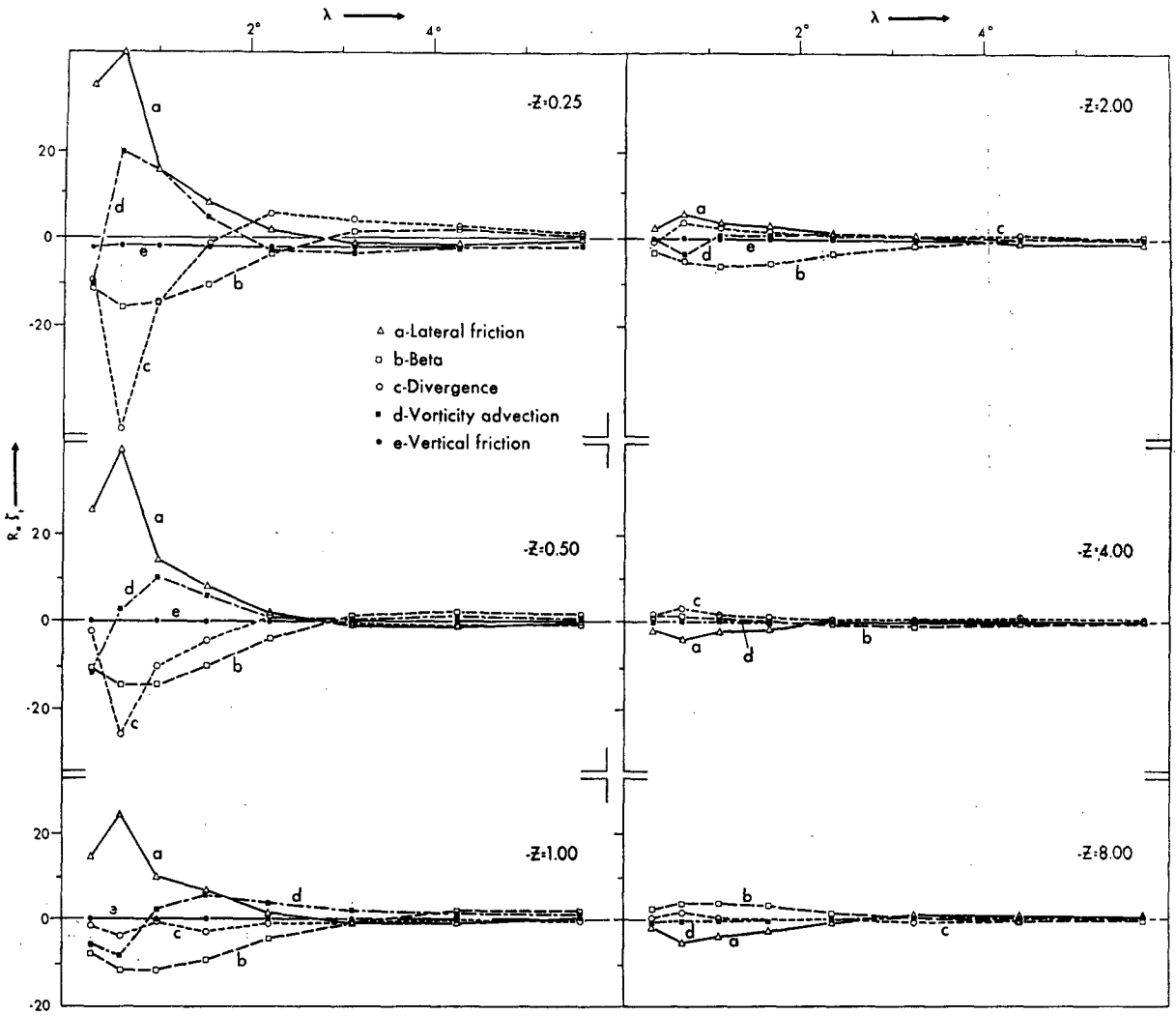


FIG. 2. The vorticity balance at the western wall for each level. The ordinate is the local vorticity change and the abscissa is distance from the wall.

effect of various terms in (3.1) for the interior region and for the western boundary current.

Turning first to the interior region, the heat balance terms are shown in Figs. 3 and 4. The vertical sections represent averages with respect to longitude for the interval $15°<\lambda<40°$. This interval excludes a 15° strip parallel to the western boundary and a 5° strip at the eastern boundary. The heat balance terms have also been averaged with respect to time over the interval shown in Fig. 6, Part I. The two horizontal advection terms in (3.1) are lumped together, while the vertical mixing term is broken down into two components. Vertical mixing for the statically stable and unstable cases are shown separately, the unstable case being labeled "convection." Since the patterns are averages with respect to space and time, both components of vertical mixing can be significant for the same points in the sections of Fig. 3.

The various terms in the heat balance are very much smaller below the thermocline than at the surface. In order to show the detail at mid-depths a logarithmic spacing is used. The three major terms $\vartheta_{zz}$ (stable), $-\mathbf{V}\nabla\vartheta$ and $-w\vartheta_z$ are shown at the top of Fig. 3. The vertical diffusion is positive over most of the section, transfering heat from the surface down into the ocean. This transfer is essential in setting up the density gradients that drive the thermohaline circulation. An exception to the general rule occurs near the surface in the 10°–20° latitude belt. In this region the wind pattern forces a strong downwelling. The effect of downwelling on the heat balance is partly balanced by negative values of the diffusion term.

Of particular interest is the field of horizontal advection shown in Fig. 3 (upper right). An analysis in the Appendix of Part I shows that difficulties occur in computing the heat advection due to the wind drift

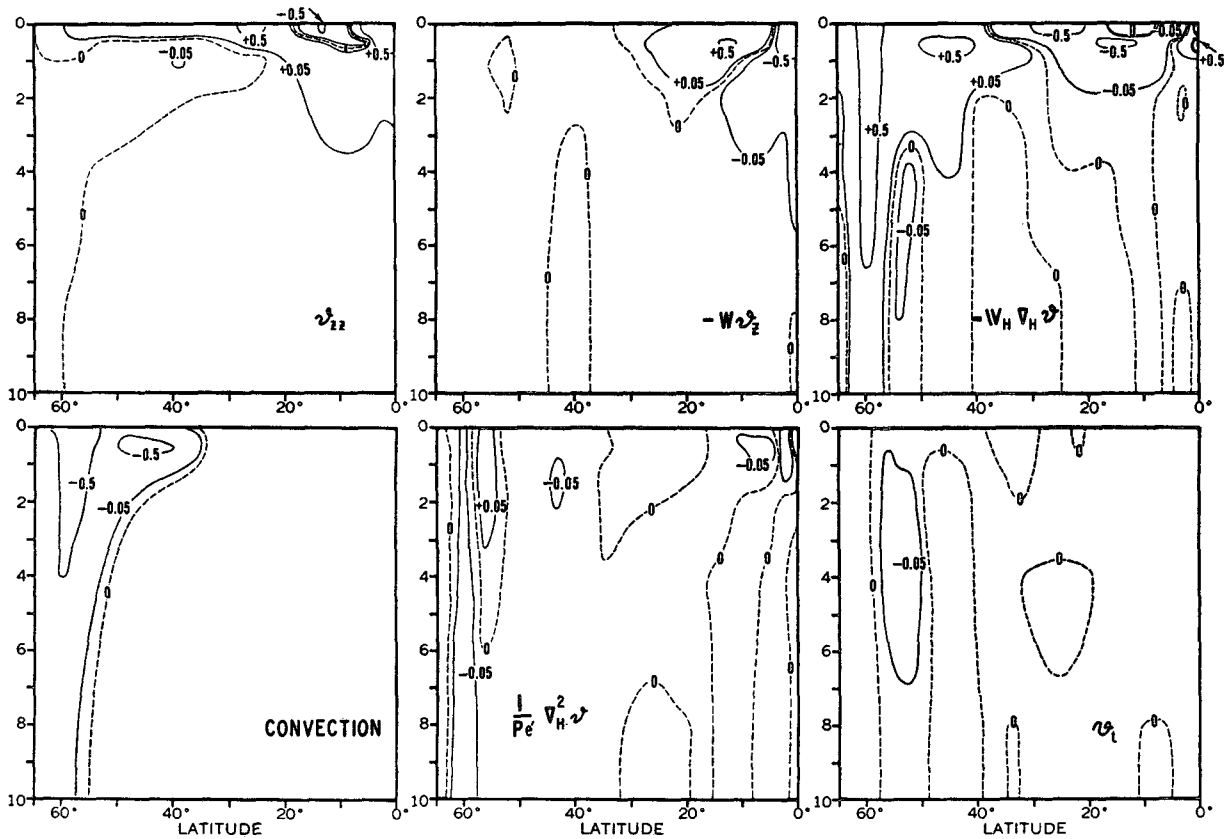


FIG. 3. The heat balance of the interior. Note the important role of horizontal advection.

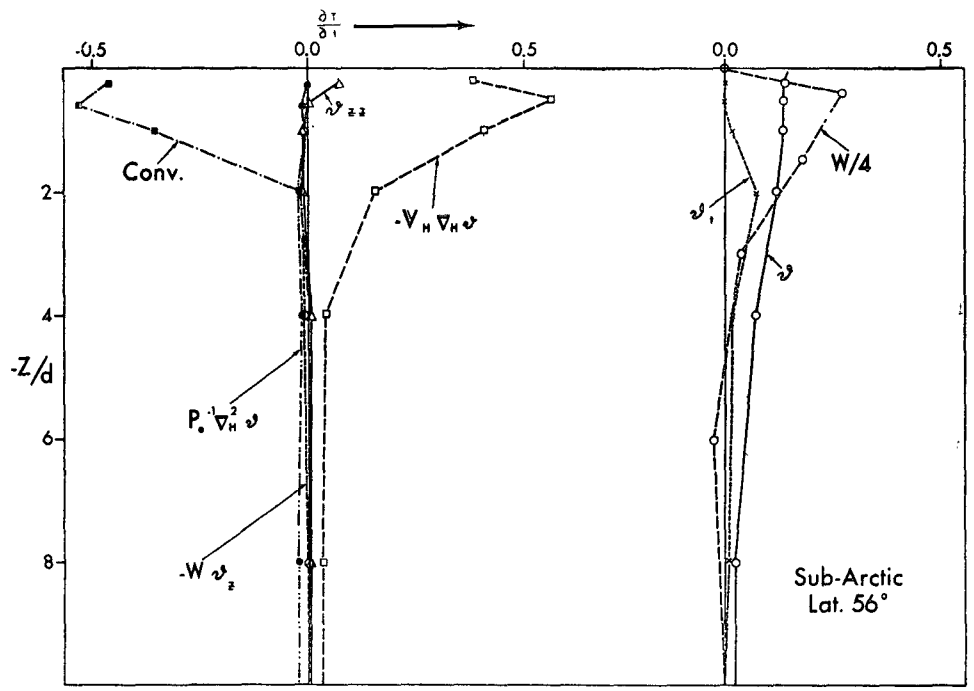


FIG. 4a. Heat balance components (left) and temperature and vertical velocity profiles (right) for the subarctic.

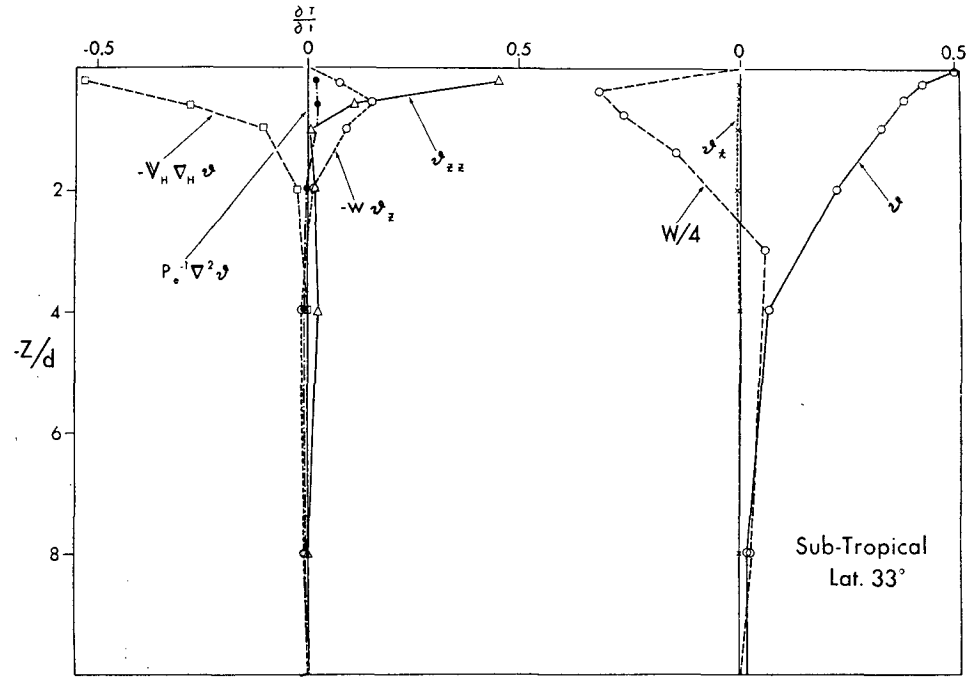


FIG. 4b. Heat balance components (left) and temperature and vertical velocity profiles (right) for the subtropics. Note the relative importance of horizontal advection.

current in the top layer where the horizontal temperature gradient changes rapidly with respect to depth. Due to very strong upwelling near the equator, a reversal of the north-south temperature gradient imposed at the surface does take place at low latitudes quite near the surface (see Fig. 10, Part I). While the validity of the horizontal advection terms in this immediate area is doubtful, this source of error is not

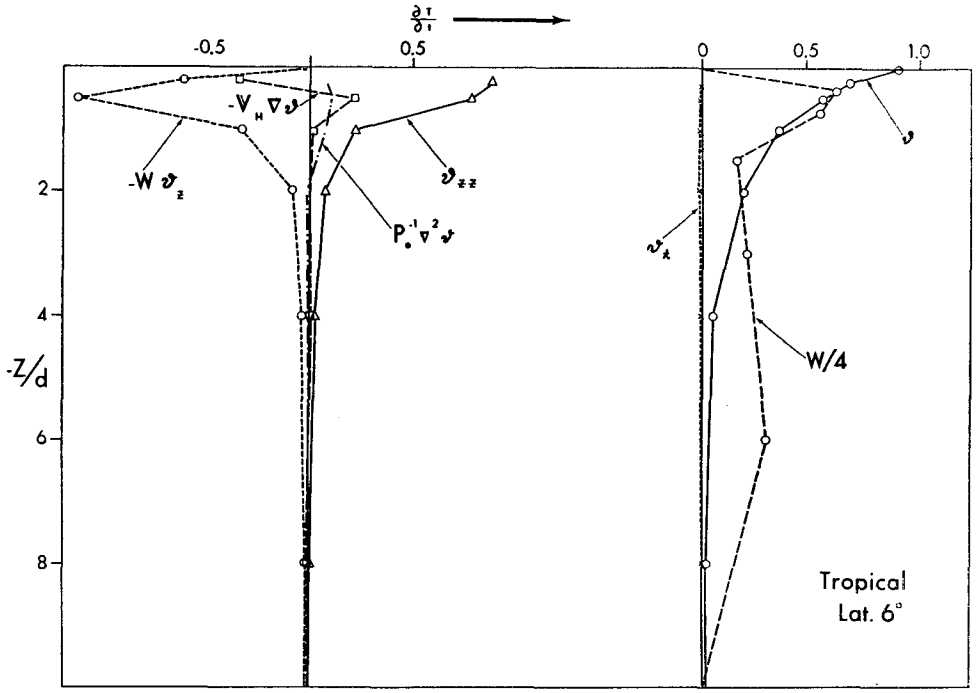


FIG. 4c. Heat balance components (left) and temperature and vertical velocity profiles (right) for the tropics.

present below the surface layer and at higher latitudes. The most striking feature shown in Fig. 3 is that horizontal advection is comparable in magnitude to the other terms in (3.1) from the surface down to the base of the thermocline. In the subtropical gyre the interior flow at upper levels is to the south, and in the subarctic gyre it is to the north. Taking into account that cold water lies to the north, it is to be expected that near the surface the horizontal advection term is positive in the subarctic gyre region and negative in the subtropical gyre.

The pattern of convection (lower left) indicates that convective overturning is confined to the northern part of the basin. Comparing the pattern of lateral advection in the northern part of the basin with the convective pattern, it is possible to see that the two terms are closely balanced. The warming caused by northward drift in the interior of the subarctic gyre is balanced by convective cooling.

No clear pattern shows up in the horizontal mixing (lower middle), which, relative to other terms, plays a smaller role. The time change of temperature shows that the system is not in complete balance over the time period considered. The largest transient appears in the north part of the basin at mid-depths. Note that this maximum in $\vartheta_t$ is closely balanced by a similar peak in the lateral advection pattern. It is probably associated with nearly barotropic, low frequency oscillations in the subarctic gyre.

A more precise picture of the heat balance is given by the profiles shown in Figs. 4a–c. The different terms of the heat equation taken from the same averages shown in the previous figure are shown as a function of depth. Also shown in Figs. 4a–c are the profiles of temperature and vertical velocity to help in the physical interpretation of the heat balance terms. As pointed out in connection with Fig. 3, the heat balance in the subarctic region mainly consists of a balance between convection and lateral advection. This is shown clearly in Fig. 4a. The stratification is too weak for vertical advection or vertical mixing to be important. At great depths there is an approximate balance between horizontal advection and horizontal mixing.

The interior heat balance in the subtropical zone is given in Fig. 4b. Note that vertical advection reverses sign quite far below the surface. It is somewhat surprising to see how deep the wind induced downwelling penetrates into the thermocline. Almost all the inflow of heat at the surface is balanced by horizontal advection. It is interesting to compare this result with thermocline theory. Based on an exact solution of the thermocline problem for a special case, Blandford (1965) found that the horizontal advection is of the same order as other factors in the thermocline. In an earlier study, however, Robinson and Welander (1963) found that advection played a quantitatively small role. The present results appear to favor Blandford's conclusions.

In the tropics vertical advection and downward diffusion dominate the heat balance. The vertical velocity shown in Fig. 4c has two maxima, the upper one apparently related to Ekman suction. The upwelling at the equator is so strong that even at the first level the coldest water lies to the south, just the reverse of the distribution given by the surface boundary condition. The surface stress in low latitudes is directed to the west. This gives rise to a northward Ekman drift, which in the continuous case would be concentrated in a very thin planetary boundary layer. The northward drift shows up very clearly in the velocity patterns of Fig. 11, Part I. In the continuous case the heat advection by the drift current would be associated with the surface temperature gradient. In the finite difference method, however, lateral advection is governed by the temperature gradient at the first level. Since the temperature gradient at the first level is opposite to that given by the surface boundary condition, the lateral advection computed by the finite difference method has the wrong sign. This error indicates that a vertical resolution adequate to resolve the thermocline in most areas may still be very inadequate to resolve the much more intense, shallow thermocline that forms in the vicinity of the equator.

The next area under consideration is the vicinity of the western wall at 28° latitude. Fig. 5 gives a complete two-dimensional picture of the heat balance. The various components of (3.1) are plotted as a function of distance from the wall for each level. At the top level, an approximate balance exists between small-scale convection and lateral advection. The shallow, but very violent, convection that goes on here is associated with the flow of warm water northward and the fact that temperature at the surface is rigidly fixed by the upper boundary condition. The importance of this feature of the model may be somewhat artificial. In the real ocean, interaction between the atmosphere and the underlying sea always takes place. Under such circumstances such violent convection in the ocean could not be maintained without a rise in the ocean surface temperature, which in turn would slow down the rate of heat transfer upward.

At the second level down from the surface, the heat balance is changed somewhat. The largest cooling effect is due to vertical advection. The boundary conditions are such that lateral advection must go to zero at the boundary, where vertical advection reaches a maximum. Very close to the wall, horizontal mixing must therefore increase rapidly to maintain a balance. At the $Z=-1.00$ level, small-scale convection disappears altogether, and the balance close to the wall must be entirely due to the combined effect of vertical advection, lateral and vertical mixing. The very strong upward motion close to the wall has already been discussed in connection with the vorticity balance in the previous section. Farther out from the wall, downward motion takes place and this is reflected in the behavior of the vertical

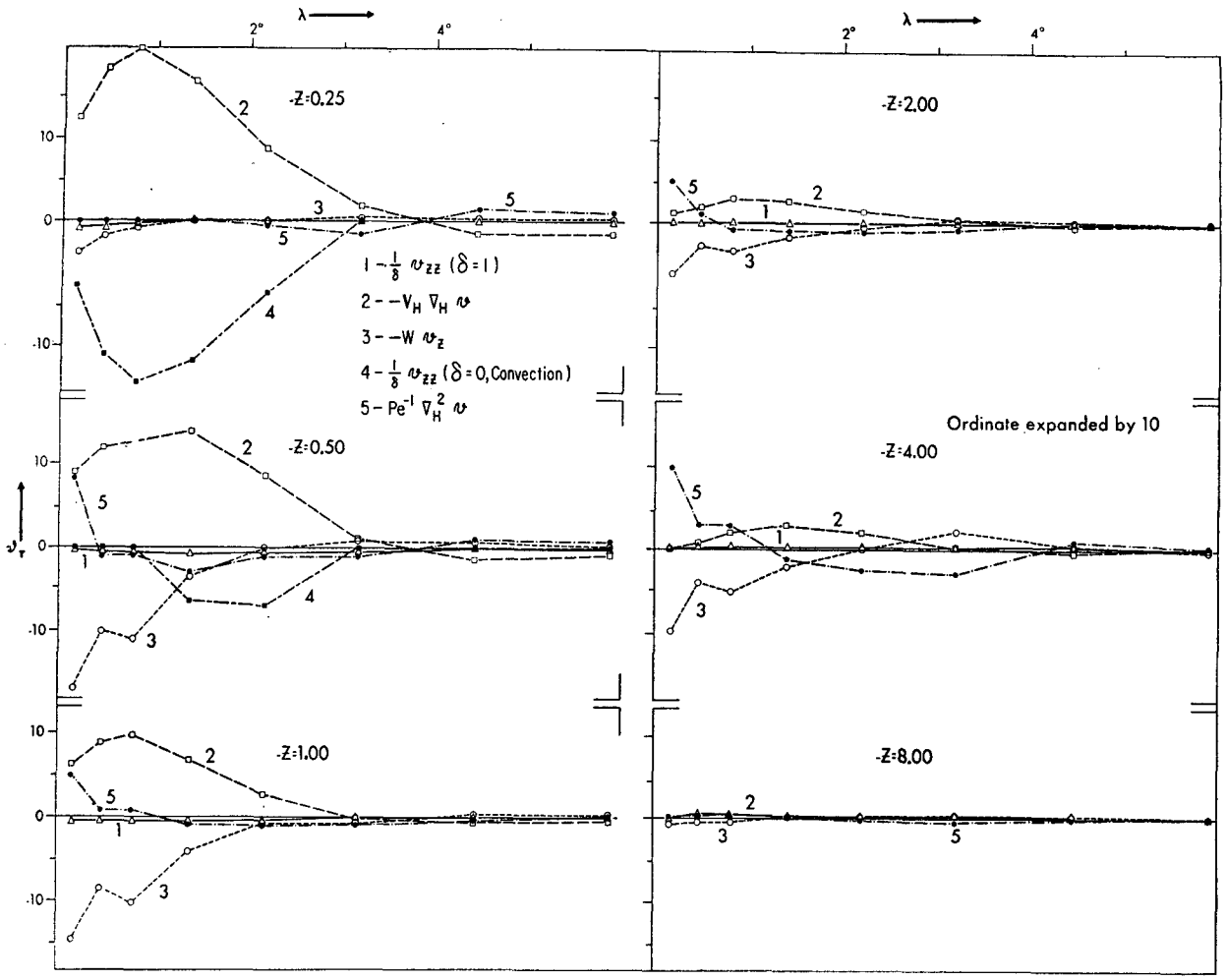


FIG. 5. Heat balance components at the western wall given at each level. Ordinate is local temperature change, and the abscissa is distance from the wall. The latitude is 28°.

heat advection term. This is particularly striking at the $Z=-4.00$ level.

The main conclusions to be drawn from Fig. 5 are: 1) the heat balance is mainly determined by lateral mixing and vertical advection in the immediate vicinity of the western wall; and 2) lateral advection tends to transfer heat from the interior region of the subtropical gyre into the western boundary current region and the tropics where it is balanced by strong upwelling and convection.

A certain amount of caution must be exercised in carrying over the ideas suggested by this solution to the real ocean. It is shown in the previous section that the strong upwelling at the western wall is connected with friction at the boundary. Since the details of friction at the lateral boundary of the real ocean must be considerably more complex than the present model, upwelling at the western boundary may also be different. Nevertheless, an interesting question is posed with respect to the real ocean: How much of the heat received at the surface in low latitudes is balanced by local upwelling associated with "planetary divergence," and how much heat is transferred laterally to distant areas where it is balanced by upwelling induced along lateral boundaries?

## 4. Energy cycle

Relatively little is known of the energy cycle of large-scale motions in the world ocean. There is no equivalent in the ocean of the radiosonde network which has permitted quite detailed analysis of atmospheric energetics. The study of theoretical ocean models may therefore be very valuable in predicting features of the energy cycle, and suggesting the most efficient observational programs for this problem. In addition, the analysis of the energy cycle indicated by the present solution provides a valuable test of the physical consistency of the method of solution, which cannot be obtained by simply examining the fields of the principal variables themselves.

For convenience, let $K$ designate the kinetic energy which will be divided into two principal components,

$$\bar{K}=\{\bar{u}^2+\bar{v}^2\}/2, \tag{4.1}$$

$$\hat{K}=\{\hat{u}^2+\hat{v}^2\}/2, \tag{4.2}$$

the braces indicating an average taken over the entire volume. The overbar, $\bar{}$, and caret, $\hat{}$, indicate a vertical average and the deviation from the vertical average as in the previous section. The equation for the change in $\bar{K}$ with respect to time is obtained directly by averaging (2.24) and (2.25) of Part I with respect to $z$ and multiplying the results by $u$ and $v$, respectively. Summing the results, we have

$$\mathrm{Ro}\bar{K}_t=I_1+I_2+I_3, \tag{4.3}$$

where

$$I_1=-\mathrm{Ro}\{\bar{u}\overline{(\mathbf{v}\nabla_2 u+wu_z)}+\bar{v}\overline{(\mathbf{v}\nabla_2 v+wv_z)}\}, \tag{4.4}$$

$$I_2=\frac{\mathrm{Ro}}{\mathrm{Re}}\{\bar{u}\overline{F^\lambda}+\bar{v}\overline{F^\varphi}\}, \tag{4.5}$$

$$I_3=\mathrm{Ro}\{\bar{u}\bar{u}_{zz}+\bar{v}\bar{v}_{zz}\}. \tag{4.6}$$

$I_1$ is the energy exchange due to the nonlinear terms. It will be shown that this leads to an exchange between the two components, $\bar{K}$ and $\hat{K}$, but no net gain or loss for the entire system. $I_2$ is the change in $\bar{K}$ due to lateral friction, and is always negative definite. The third term is the contribution of vertical diffusion.

Since

$$\bar{u}_{zz}=\frac{d}{H}\int_{-H/d}^{0}u_{zz}dz=\frac{d}{H}\tau^\lambda \tag{4.7}$$

in the absence of bottom friction,

$$I_3=\mathrm{Ro}\{\bar{u}\tau^\lambda+\bar{v}\tau_\varphi\}d/H. \tag{4.8}$$

Turning now to the consideration of the other component of kinetic energy,

$$\mathrm{Ro}\hat{K}_t=I_4+I_5+I_6+I_7, \tag{4.9}$$

where

$$I_4=-\mathrm{Ro}\{\hat{u}(\mathbf{v}\nabla_2 u+wu_z)+\hat{v}(\mathbf{v}\nabla_2 v+wv_z)\}, \tag{4.10}$$

$$I_5=-\{\hat{u}mp_\lambda+\hat{v}p_\varphi\}, \tag{4.11}$$

$$I_6=\frac{\mathrm{Ro}}{\mathrm{Re}}\{\hat{u}F^\lambda+\hat{v}F^\varphi\}, \tag{4.12}$$

$$I_7=\mathrm{Ro}\{\hat{u}u_{zz}+\hat{v}v_{zz}\}. \tag{4.13}$$

Discussing these terms in order, we see that the first term is connected with nonlinear advection. We note that the sum of $I_1$ and $I_4$ may be written as

$$I_1+I_4=\left\{\mathbf{v}\cdot\nabla_2\left(\frac{u^2}{2}+\frac{v^2}{2}\right)+w\left(\frac{u^2}{2}+\frac{v^2}{2}\right)_z\right\}. \tag{4.14}$$

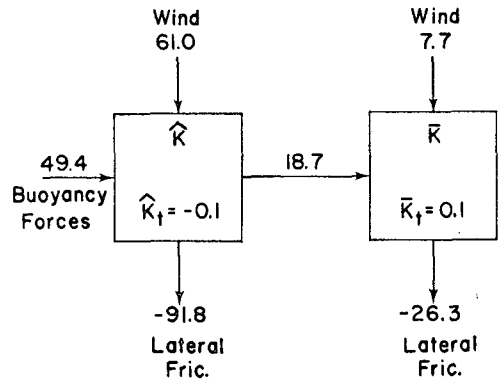


FIG. 6. Energy cycle showing the link between the kinetic energy of the vertically averaged flow and the baroclinic component of the kinetic energy.

Since normal flow vanishes at all boundaries, the volume integral on the left also vanishes, and

$$I_1=-I_4. \tag{4.15}$$

Ordinarily, theoretical oceanographers think of the vertically averaged component of motion as being primarily driven by wind stresses imposed at the surface. We see here that nonlinear advection terms may provide an additional driving force by linking the $\bar{K}$ and $\hat{K}$ components of flow.

$I_5$ represents the work done by pressure forces, and is therefore the link between potential and kinetic energy. Kinetic energy is generated if there is a net correlation between vertical motion and apparent temperature over the entire system.

$I_6$ is the dissipation of $\hat{K}$ due to the lateral mixing processes. The last term on the right-hand side of (4.9), $I_7$, includes both the effect of wind stress acting near the upper surface, and the dissipation associated with vertical mixing of the $\hat{u}$, $\hat{v}$ components at depth.

The energy cycle averaged over the period, $22.32<t<22.45$ is given in a box diagram of Fig. 6, the direction of flow being indicated by arrows. This diagram shows at a glance the importance of various processes in the balance of kinetic energy. The energy $\hat{K}$ of the internal mode is maintained by roughly equal contributions of mechanical and thermal driving. The positive contribution of the buoyancy forces means that on the average upward motion coincides with less dense water and *vice versa*. Further investigation is needed to determine if this result is valid when the Rossby number is reduced from the present value of $2\times10^{-4}$ to a more realistic value of $2\times10^{-5}$. Calculations (unpublished) made in connection with study A (Bryan and Cox, 1967) show that the buoyancy forces may become negative as the rotational constraint is increased.

Over 80% of the energy received in the $\hat{K}$ box is directly disspated by lateral friction. The remainder is passed to the external mode component $\bar{K}$ of the kinetic energy. Note that this nonlinear energy transfer

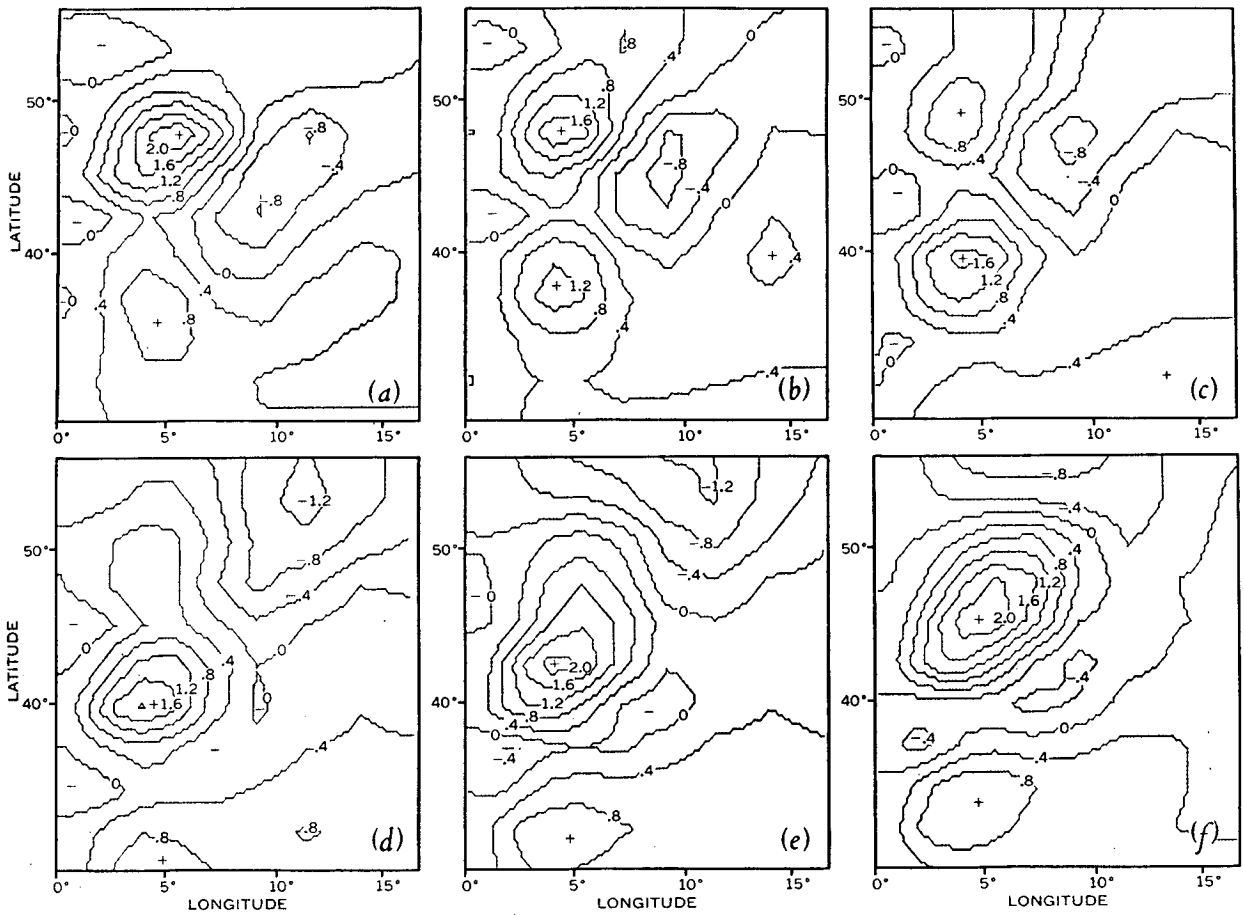


FIG. 7. Patterns of the mass-transport stream function showing the growth and movement of disturbances in the western boundary current region. The patterns are taken at intervals of approximately 2/100 of a time unit.

term, $I_4$, is over twice as large as the direct driving of the wind in maintaining the $\bar{K}$ component. As discussed in Part I some of the results of the conventional wind-driven ocean theory break down when nonlinear terms are introduced. Linear theory gives a direct relationship between the amplitude of the total transport (the external mode) and the driving force of the wind. The results of Part I show that the actual amplitude of the external mode in the present case is almost twice that given by linear theory. The energy diagram given in Fig. 6 suggests that this increase in amplitude is definitely required to give a dissipation large enough to balance the additional contribution of energy due to the nonlinear transfer of energy from the internal mode of motion.

## 5. Time-dependent motion

In Part I it is noted that important time-dependent motions are found in the solution. Examination of the patterns of mass transport indicate three main categories of fluctuations with quite different frequencies. The highest frequency fluctuations are regular disturbances in the mass-transport pattern moving from east to west in the subtropical gyre. The period of these moving disturbances agrees almost exactly with the period of Rossby waves in a barotropic, $\beta$-plane ocean (Phillips, 1966).[1] These disturbances extend only up to a latitude of 50°. The lowest frequency disturbances appear in the upper part of the basin north of this limit. Swirls appear in the mass-transport pattern. These swirls have no apparent organized movement to the east or west, but slowly grow and decay with periods of $\frac{1}{4}$–$\frac{1}{2}$ time unit.

Of greatest interest are small scale disturbances imbedded in the western boundary current. Synoptic patterns of the stream function in the region just adjacent to the western boundary are shown in Fig. 7. These synoptic patterns form a series taken over the averaging interval defined in Part I. In the first pattern an intense gyre is shown in the upper part of the area. In the following patterns this gyre gradually weakens and a new gyre is swept upstream, gradually increasing in amplitude. Finally, the new gyre stagnates in nearly the same position as the first intense gyre. In the final

[1] It has been brought to the authors' attention that the first derivation is due to Høiland (1950, see pp. 24–25).

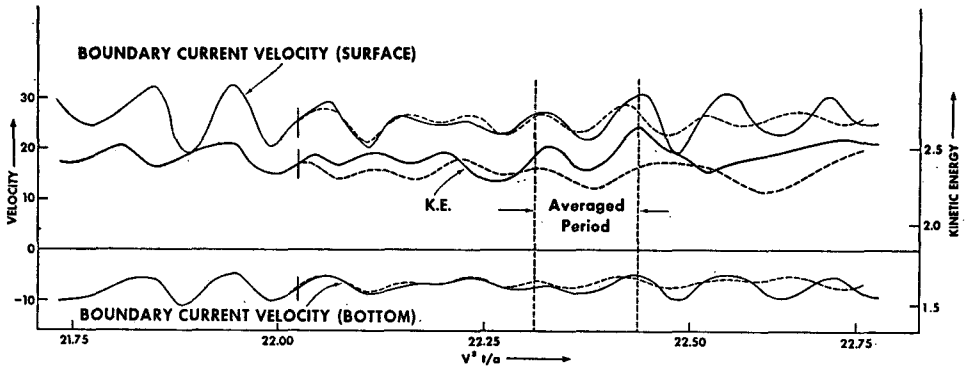


FIG. 8. The time-dependent behavior of the velocity of the western boundary current and the kinetic energy. The dashed curves give the results for a separate run including bottom friction.

pattern it is possible to see a third nascent disturbance ready to move upstream.

The transport of the western boundary current given by linear theory is 0.8 nondimensional units (see Section 5, Part I). The disturbances have a very large amplitude, nearly twice this value. Except for this very large amplitude, there are many similarities between these disturbances and those found in computations made for a barotropic model (Bryan, 1963). In the barotropic model the traveling disturbances only appeared as the Reynolds number was increased, and appeared to be generated by shear flow instability.

The $V$ component in the western boundary is shown as a function of time in Fig. 8. Curves are shown for both the surface and bottom velocity. The roughly parallel behavior of the surface and bottom velocity indicates that the traveling disturbances are largely barotropic. The total kinetic energy curve (solid line, Fig. 8) is roughly correlated with the velocity curve, indicating the importance of the western boundary current in determining the total energy of the entire basin. The dashed lines in Fig. 8 are for a special computation which includes bottom friction. The formulation given in Part I is based on Ekman theory, and the same level of vertical mixing as used throughout the study. The curves indicate that the general intensity of the circulation as measured by the strength of the western boundary current does not change very much when bottom friction is included. The most interesting difference is a very slow damping of the disturbances. Since the disturbances extend right to the bottom, one might anticipate that bottom friction would have this effect.

To investigate the traveling disturbances further, a computation is made of the Reynolds stresses at three latitudes, along lines cutting across the western boundary current. If we let

$$\alpha=\bar{\alpha}+\alpha', \quad \bar{\alpha}=\frac{1}{\Delta t}\int_0^{\Delta t}\alpha dt,$$

and apply this same bar operator to the momentum equation for the $V$ component, we have

$$\mathrm{Ro}(\bar{v})_t=-\mathrm{Ro}\sec\varphi(\overline{u'v'})_\lambda+\cdots.$$

The term on the right-hand side is the gradient of one of the Reynolds stress components. The remaining terms in the equation have been omitted. The term on the right is found to be negative for all three sections considered. This indicates that the eddies act like friction and tend to retard the time-averaged flow of the boundary current. In an observational study near Cape Hatteras, Webster (1961) found the opposite to be true for the Gulf Stream. This difference between model and prototype poses an interesting problem which cannot be explained on the basis of existing theories of the Gulf Stream.

## 6. Summary and conclusions

An analysis of the vorticity balance of the subtropical gyre region shows very large differences between the highly geostrophic flow of the interior, and the quasi-geostrophic flow at the western boundary. Vertical motion in the interior is almost entirely explained by the "planetary divergence" associated with the latitudinal variation of the Coriolis parameter. On the other hand, the divergence in the western boundary current is largely balanced by lateral friction. Near the surface, inertial effects tend to combine with lateral turbulent diffusion to transfer cyclonic vorticity generated at the western wall out into the main body of the fluid.

The heat balance of the interior region, away from the western wall, is analyzed in some detail. Based on a thermocline calculation without wind, Robinson and Welander (1963) have concluded that horizontal heat advection has a relatively small effect. On the other hand, the present calculations indicate that horizontal advection is of the same order as other terms at the surface and through most of the thermocline. An analysis of the heat balance of the western boundary current shows that heat received from the interior of the subtropical gyre by horizontal advection is balanced

by convective mixing through the upper surface, and in deeper layers by cold upwelling adjacent to the wall.

An analysis of the total energy cycle of the flow indicates that work done by wind is of the same order as the work done by buoyancy forces in generating motion. An energy transfer through the inertia terms links the kinetic energy of the vertically averaged flow to the baroclinic component. Qualitatively, about half of the total dissipation in the kinetic energy of the vertically averaged flow is compensated for by work done by wind, the remainder by the inertial link with the baroclinic part of the flow.

Compared with the present case the theory of a barotropic wind-driven ocean seems very simple. In the barotropic theory only a linear interior regime and a viscous-inertial regime at the western boundary have to be considered. The baroclinic case, on the other hand, requires the consideration of many more boundary regimes. In addition, the interior regime is much more complex. Many more numerical and analytic studies will probably be required to gain an understanding of the details of each of these boundary regimes and how they interact with the interior flow. In particular, efforts should be made to carry out calculations with much greater vertical resolution in the numerical net. The effect of a bottom Ekman layer should also be explored more fully. In the way of analytic studies, an extension of the thermocline theory would be very useful in interpreting the present results. The principal requirement is to adapt the thermocline solutions to take into account an ageostrophic layer at the eastern wall. An analytic approach would also be useful for shedding some light on the complicated time-dependent motions found in the present calculations.

The effort required to carry out future studies of this kind is well justified by the very great range of applications of similar numerical models of ocean currents. With the addition of a more detailed formulation of turbulence for the ocean, and a realistic geometry, a powerful tool will become available for analyzing field observations made by oceanographic vessels, calculating the movement of tracers in the ocean, and predicting the large-scale response of the ocean to changing meteorological conditions.

## REFERENCES

Blandford, R., 1965: Notes on the theory of the thermocline. *J. Marine Res.*, **23**, 18–29.

Bryan, K., 1963: A numerical investigation of a nonlinear model of a wind-driven ocean. *J. Atmos. Sci.*, **20**, 594–606.

——, and M. D. Cox, 1967: A numerical investigation of the oceanic general circulation. *Tellus*, **19**, 54–80.

——, and ——, 1968: A nonlinear model of an ocean driven by wind and differential heating: Part I. Description of the three-dimensional velocity and density fields. *J. Atmos. Sci.* **25**, 945–967.

Høiland, E., 1950: On horizontal motion in a rotating fluid. *Geofys. Publikasjoner*, **17**, No. 10, 26 pp.

Phillips, N. A., 1966: Large-scale eddy motion in the western Atlantic. *J. Geophys. Res.*, **71**, 3883–3891.

Robinson, A. R., and P. Welander, 1963: Thermal circulation on a rotating sphere with application to the oceanic thermocline. *J. Marine Res.*, **21**, 25–38.

Webster, F., 1961: The effect of meanders on the kinetic energy balance of the Gulf Stream. *Tellus*, **13**, 392–401.